Analytica Chimica Acta 933 (2016) 89–96

Contents lists available at ScienceDirect

Analytica Chimica Acta

journal homepage: www.elsevier.com/locate/aca

Enzymatic biosensor of horseradish peroxidase immobilized on Au-Pt nanotube/Au-graphene for the simultaneous determination of antioxidants

Long Wu [1], Wenmin Yin [1], Kun Tang, Dian Li, Kang Shao, Yunpeng Zuo, Jing Ma, Jiawei Liu, Heyou Han*

State Key Laboratory of Agricultural Microbiology, College of Food Science and Technology, College of Science, Huazhong Agricultural University, Wuhan 430070, PR China

HIGHLIGHTS

- SAP NTs was synthesized and demonstrated to exhibit intrinsic peroxidase and catalase-like activity.
- The structure of SAP NTs provides larger surface area and more favorable medium for electron transfer.
- Horseradish peroxidase immobilized on Au-Pt nanotube/Au-graphene acted as enzymatic biosensor.
- The simultaneous detection of BHA and PG in food matrices was achieved based on enzymatic biosensors.

GRAPHICAL ABSTRACT

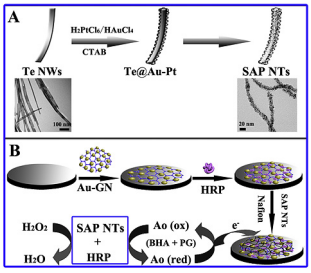

ARTICLE INFO

Article history:
Received 27 April 2016
Received in revised form
7 June 2016
Accepted 16 June 2016
Available online 21 June 2016

Keywords:
Enzymatic biosensors
Horseradish peroxidase
Spiny Pt-Au nanotube
Antioxidants
Linear-sweep voltammetry

ABSTRACT

A new electrochemical method has been proposed for the simultaneous determination of butylated hydroxyanisole (BHA) and propyl gallate (PG) in food matrices based on enzymatic biosensors. Spiny Au-Pt nanotubes (SAP NTs) was first synthesized and demonstrated to exhibit intrinsic peroxidase and catalase-like activity. The structure of SAP NTs provides large surface area and favorable medium for electron transfer, on which HRP were immobilized and acted as enzymatic biosensor for the simultaneous detection of BHA and PG. The results revealed that BHA and PG both have well-defined oxidation waves with peak potentials of 624 and 655 mV, respectively. Under the optimal conditions, the method behaved satisfactory analytical performance towards BHA and PG with a wide linear range of 0.3 −50 mg L^{-1} and 0.1−100 mg L^{-1}, as well as a detection limit of 0.046 mg L^{-1} and 0.024 mg L^{-1} (3σ/slope), respectively. Besides, the proposed method exhibits good sensitivity, stability and reproducibility, providing an alternative to fabricate electrode and construct sensitive biosensors.

1. Introduction

Antioxidants, a group of synthetic or natural substances added to products, can prevent or delay their deterioration by the oxygen in air. In food matrix, antioxidants have attracted broad interests in slowing down the adverse effects of reactive species, such as reactive oxygen (ROS) and nitrogen species (RNS), and thus extend

* Corresponding author.
E-mail address: hyhan@mail.hzau.edu.cn (H. Han).
[1] Equal contribution.

http://dx.doi.org/10.1016/j.aca.2016.06.020
0003-2670/

the shelf-life of foods [1,2]. Due to some of their advantages, such as chemical stability, availability and low cost, synthetic food antioxidants are more extensively used than natural antioxidants [3]. These synthetic antioxidants are mainly phenolic compounds, including butylated hydroxyanisole (BHA), *tert*-butylhydroquinone (TBHQ), propyl gallate (PG) and butylated hydroxytoluene (BHT). Generally, they are widely used in food, pharmaceutical and other commercial products such as oils or fats, and lubricants [4]. However, it was reported that the excess use of synthetic antioxidants in foodstuff may cause a loss of nourishment, and even produce toxic effects [5,6]. For example, BHA may play a role in liver damage and carcinogenesis in laboratory animals and PG is carcinogenic to mice and rats [7,8]. The use of these antioxidants was strictly regulated in many countries [9,10]. Thus, it is important to quantify the synthetic antioxidants (e.g. BHA and PG) in food for the sake of human health, food safety and foodstuff production [11,12].

To determine the synthetic antioxidants in various matrices, many analytical methods have been proposed, such as high performance liquid chromatography with fluorescence detector (HPLC–FLD), gas chromatography, liquid chromatography, and spectrophotometry [13–16]. Although these methods are widely used and behave unique advantages, they are usually confronted with difficulties of labor-intensive or time-consuming. Hence, it is of great importance to develop a convenient method for the determination of these antioxidants. Up to now, electrochemical method has been widely applied in medical, biological, and environmental analysis [17,18]. Because of its simple operation, high sensitivity and rapid response, this method has become a widely accepted approach to determine the synthetic antioxidants [19,20]. Wherein, biosensors coupled with enzyme are usually constructed in the development of electroanalytical methods [21,22]. The biosensors convert biological information to electrical signals via a molecular reaction on a physical transducer by giving quantitative analytical information of the analyte [23,24]. However, it is a challenge to improve the electron transfer between active site of the enzyme and electrode.

Owing to its excellent physical and electrical properties, graphene nanosheet has aroused great attention and interests in experimental and theoretical communities [25,26]. In addition, intensive efforts have been made in developing nanoparticles modified graphene. Wherein, gold nanoparticles modified graphene (Au-GN) has been widely used in electrochemical analysis due to the advantages such as catalysis, high effective surface area and regulate and control over electrode microenvironment [27]. On the other hand, metallic alloy NPs play an important role in the field of catalysis and sensors because of their better catalytic properties compared with the monometallic counterparts [28,29]. Among the bimetallics, Au-Pt is one of the most popular bimetallic nanoparticles that has been extensively applied in electrochemistry [30]. Taking into the above advantages consideration, it would be an effective way to combine spiny Au-Pt nanotubes (SAP NTs) with HRP as biosensors for particular electrochemical analysis.

In this work, we designed a novel enzyme biosensor based on SAP/HRP/Au-GN composites for the simultaneous determination of BHA and PG (see Scheme 1). As shown in Scheme 1B, the Au-GN hybrids were first modified on the carbon electrode to accelerate the electron transfer rate and amplify the electrochemical signal. Afterwards, HRP enzyme was decorated onto the electrode through electrostatic attraction. Finally, the spiny Au-Pt nanotubes were decorated on Au-GN hybrids to produce a dimensional network nanostructure. The hierarchical web-like structure further accelerated the electron transfer and provided a platform for the entrapment of HRP. Thus, HRP enzyme was immobilized onto the electrode with the help of Au-GN hybrids and APS NTs. Satisfactory

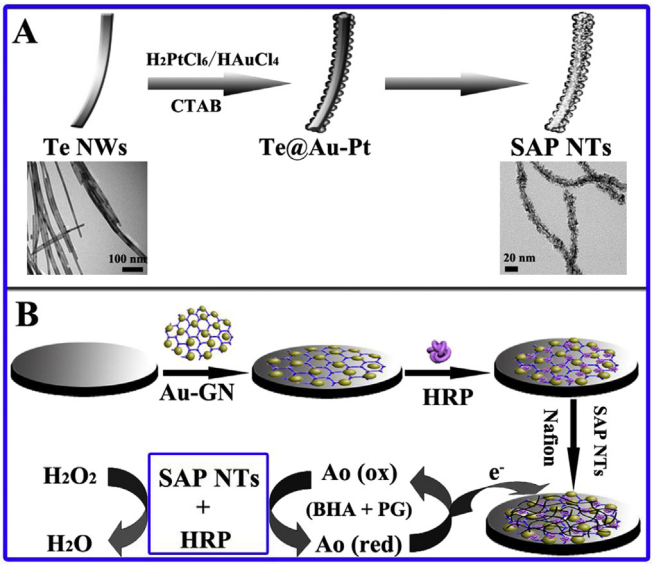

Scheme 1. Illustration for the preparation of SAP NTs **(A)** and the construction of enzymatic biosensors for the simultaneous detection of the antioxidants (Ao: BHA and PG) **(B)**.

results for the simultaneous determination of BHA and PG were obtained by LSV. Besides, the proposed SAP/HRP/Au-GN sensors exhibit enhanced electrochemical properties in sensitivity, stability and reproducibility, suggesting their potentials in electrochemical analysis.

2. Experimental

2.1. Reagents and chemicals

BHA, BHT, PG, TBHQ, Bisphenol (BPA), Hexadecyl trimethyl ammonium bromide (CTAB, 99%), sodium dodecyl sulfate (SDS, 99%) were purchased from Sigma-Aldrich. Tellurium dioxide powder (TeO_2, 99.99%) was purchased from Aladdin Chemistry Co., Ltd. Hydrazine monohydrate (85%, AR), tetrachloroauric(III) acid hydrate ($HAuCl_4 \cdot 4H_2O$, AR), chloroplatinic acid hexahydrate ($H_2PtCl_6 \cdot 6H_2O$, AR), 3, 3′, 5, 5′-tetramethylbenzidine (TMB), sodium hydrate (NaOH, AR) and other relevant reagents were supplied by Sinopharm Chemical Reagent Co., Ltd. Ultrapure water obtained from a Millipore water purification system (Milli-Q, Millipore, 18.2 MΩ resistivity) was used throughout the experiment.

2.2. Instruments

Electrochemical measurements were performed by an electrochemical work station (CHI660D Instruments, Shanghai Chenhua Instrument Corp., Shanghai, China) with conventional three-electrode system. An Ag/AgCl (saturated KCl) electrode was used as a reference electrode. The UV–vis absorption spectra were obtained on Nicolet Evolution 300 UV–vis spectrometer (Thermo Nicolet, America); Hydrodynamic diameters were performed Malvern Zetasizer Nanoseries (Malvern, England) with 633 nm laser excitation at 25 °C. An Aglient, Eclipse XDB-C18 column, 4.8 × 150 mm, 5 μm particle size was used in HPLC tests. The energy-dispersive X-ray spectroscopy (EDS) analysis was done by a JEM-2010FEF transmission electron microscope with an EDAX attachment operating at an accelerating voltage of 200 kV. Transmission electron microscopy (TEM) and high-resolution transmission electron microscopy (HRTEM) measurements were made

on a JEM-2010FEF high-resolution transmission electron microscopy at an accelerating voltage of 200 kV. The compositions of Pt nanomaterials were determined by ICP–AES (ELAN 6000, Perkin-Elmer). The X-ray diffraction (XRD) analysis was performed on a Bruker D8 Advance X-ray diffractometer with Cu Kα radiation.

2.3. Preparation of Au-GN hybrids

Au NPs and PDDA-capped graphene nanosheets (PDDA-GN) were synthesized according to the previous methods with some modification [31,32]. The details are described in Supporting Information.

2.4. Preparation of Te nanowires

Te NWs were prepared according to the previously reported methods with some modifications. First, 0.16 g of TeO_2 powder was added into a reaction bottle, then 5 mL of the preheating $N_2H_4 \cdot H_2O$ (40 °C) was added into the reaction bottle under constant magnetic stirring. The color of the solution changed from off-white to fulvous and then to bluish-violet with a resulting color of purple-black after 10 min. Second, to obtain well-defined TeNWs, 0.2 g of SDS (14 mM) was mixed with the as-prepared solution and stirred at 40 °C for another 10 min. Finally, Te NWs were obtained by centrifuging the mixture solution at 11500 rpm for 20 min and the precipitation were re-suspended in 9 mL of water and stored at 4 °C for use.

2.5. Synthesis of spiny Au-Pt nanotubes

In the typical synthesis, 1 mL the above obtained TeNWs was dispersed in 6 mL of CTAB solution (1 mM) under constant magnetic stirring for 10 min. After that, 650 μL of H_2PtCl_6 (1 mM, pH = 7.0) with 0.1 M NaOH was added to the mixture and stirred for 5 min, followed by the addition of another 400 μL of H_2PtCl_6 (1 mM). After 20 min, 600 μL of $HAuCl_4$ (1 mM, pH 7.0) with 0.1 M NaOH was introduced to the solution under constant magnetic stirring. The color of the solution changed from blue to amber after 5 min. Finally, the spiny Au-Pt nanotubes were washed several times by centrifuging the mixture solution at 11500 rpm for 10 min and the precipitation were re-suspended in 1 mL of water for further use.

2.6. Fabrication of modified electrode

The pretreatment of glass carbon electrode (GCE) was firstly carried out by polishing with alumina slurries and sonicating with ethanol and water, successively. After that, GCE was dried under nitrogen atmosphere and modified by dropping 10 μL of Au-GN dispersion (0.1 mg mL^{-1}) and dried at room temperature [33]. Then the modified electrode was immersed into 0.1 M phosphate buffer solution (PBS, pH = 9.0) containing 5 mg mL^{-1} HRP for 12 h at 4 °C. At this pH, HRP (pI ~ 7.2) bears a negative surface charge, and the modified electrode bares a positive surface charge. Finally, another 10 μL of SAP solution (4.5 mM) was dropped onto the electrode to obtain HRP/Au-GN hybrids via electrostatic attraction and van der Waals forces [34]. Thus, the HRP can be absorbed through electrostatic attraction and further trapped on the modified electrode surface and formed the SAP/HRP/Au-GN/GCE (Scheme 1B). The LSV measurements were performed in Britton–Robinson (B-R) buffer solution (pH = 2) using three electrodes [35]. The modified electrode was rinsed carefully with water before use. For comparison, bare GCE, Au-GN/GCE and HRP/Au-GN/GCE electrodes were also prepared with the same method. The as-prepared electrodes were stored at 4 °C when not in use.

2.7. Electrochemical measurements for BHA and PG

To obtain the linear calibration curves of BHA and PG, the SAP/HRP/Au-GN/GCE electrode was immersed into a standard sample solution with a certain concentration of BHA and PG, respectively. The cyclic voltammogram (CV) and LSV were both recorded by cycling the potential between +0.1 V and +0.8 V at a scan rate of 100 mV s^{-1}. The electrochemical impedance spectroscopy (EIS) was performed in the solution of 0.5 M KCl containing 5 mM $K_3[Fe(CN)_6]$ at the formal potential of 0.3 V with a frequency range of 1–10^5 Hz and a signal amplitude of 5 mV. The details of measurements were described in Supporting Information.

2.8. Treatment of food samples

In this experiment, two kinds of food matrices (oil and solid) were chosen as real samples to conduct LSV tests. Specifically, olive and peanut oils were acted as oil food simulants, and potato chips and cookies as solid food samples. All the samples were extracted using the conventional direct extraction method [6,31]. The detailed procedures are available in Supporting Information.

3. Result and discussion

3.1. Characterizations

Au-GN and spiny Au-Pt nanotubes (SAP) were firstly prepared with good uniformity and stability as mentioned above. Then the materials were assembled on the electrode layer by layer via electrostatic attraction and van der Waals forces. The fabrication processes were investigated by UV–vis absorption spectra, DLS, TEM, SEM, EDX, XPS, and HAADF-STEM.

UV–vis absorption spectra and DLS were first used to investigate the performance of Au NPs, GN, Au-GN hybrids, SAP NTs, HRP, SAP/HRP/Au-GN NCs. As depicted in Fig. S1A, the citrate stabilized AuNPs (curve a) behaved a strong characteristic absorption peak located at 508 nm, which was consistent with the local plasmon resonance of Au NPs. Meanwhile, PDDA-GN appeared a strong absorption peak at 270 nm (curve b) due to the $\pi \rightarrow \pi^*$ transitions of aromatic C=C bond. After Au NPs combined with GN, the characteristic peak of Au NPs (curve c) was shifted to 530 nm, suggesting the adsorption of Au NPs onto the nanosheets surface. SAP NTs (curve d) hardly exhibited characteristic adsorption peak and HRP enzyme (curve e) showed a characteristic Soret absorption band at 403 nm which was consistent with the previous work [36]. SAP/HRP/Au-GN NCs (curve f) behaved obvious adsorption peak located at 403 nm indicating the entrapment of HRP. Fig. S1B described the zeta potential in different modification steps. It is noteworthy that the zeta potential of GN decreased dramatically from 28.45 to 10.67 mV after combined with Au NPs. Then the zeta potential of Au-GN hybrids further decreased from 10.67 mV to −2.36 mV when combined with HRP and SAP NTs, revealing the successful self-assembly of Au-GN, HRP and SAP.

TEM images were also taken to characterize the feature of Te nanowires, Au-GN hybrids, SAP NTs, SAP/Au-GN, SAP/HRP/Au-GN NCs. As depicted in Fig. 1A, Te nanowire (Te NWs) showed a uniform nano-wire structure with an average size of 20 nm. It can be seen form Fig. 1B that Au-Pt NTs possessed an excellent structure with a narrow size distribution (~22 nm). From the HRTEM image shown in Fig. 1C, it is clear that the Au-Pt NTs are provided with spiny and porous structures. To further verify the dispersibility of Au-GN hybrids, typical TEM image of PDDA-GN (Fig. 1D) deposited with Au NPs was taken to demonstrate the homogeneous distribution of Au NPs on the PDDA-GN. It was observed that the corrugated Au-GN hybrids behaved good dispersity and the GN was

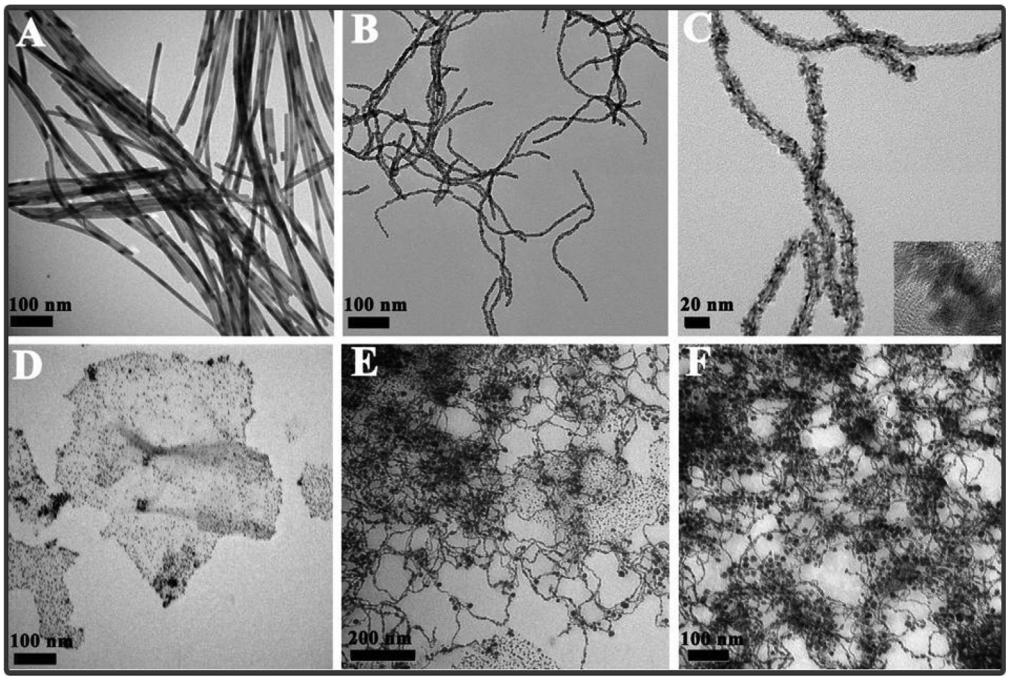

Fig. 1. TEM images of **(A)** Te NWs, **(B)** SAP NTs, **(C)** a magnified version of SAP NTs, **(D)** Au-GN hybrids, **(E)** SAP/Au-GN NCs, and **(F)** SAP/HRP/AG NCs.

dotted with AuNPs with negligible nanoparticle agglomeration. Fig. 1E showed the results after SAP mixed with Au-GN, indicating the criss-crossing distribution of SAP NTs on Au-GN. However, the distribution was more obvious when HRP enzyme was introduced as shown in Fig. 1F. This may contribute to the electrostatic attraction in the self-assembly process of SAP/HRP/Au-GN NCs.

The features could also be distinguished clearly through the surface identification of SEM (see Fig. S2A and B). Besides, the energy-dispersive X-ray spectroscopy (EDX) spectrum (Fig. S2C) was adopted to explore the component of SAP NTs. Two main peaks (Au and Pt) were observed, indicating that the SAP NTs were made up of metallic gold and platinum. Furthermore, XRD was also used to elucidate the structure formation of Au-Pt NTs. Fig. S2D shows XRD patterns Au-Pt NTs, the diffraction peaks at 39.6 and 46.3 can be assigned to the (111) and (200) face-centered cubic (fcc) structure of Pt, and the peaks at 38.2 can be ascribed to the (111) fcc structure of Au. Moreover, HAADF-STEM mapping measurements (Fig. 2A–E) were performed to monitor the Au and Pt element distribution in the nanotubes. The element mappings showed that Au and Pt are homogeneously mixed in the nanotubes. The binding energies of Pt 4f and Au 4f from Au-Pt NTs were 71.1 eV and 83.5 eV (see Fig. S3), which is in accordance with pure Pt (71.2 eV) and Au (84.0 eV). The results revealed that the Au-Pt NTs may behave a core/shell structure with segregated Au on the surface [37].

3.2. Optimisation of the experimental conditions

In the proposed method, different conditions were carefully investigated, such as pH of the electrolyte support, the concentration of HRP, SAP NTs and H_2O_2, and the scan rates (v), to obtain the best experimental working conditions. The studies were performed using 5 mg L^{-1} PG in Britton–Robinson (B-R) buffer solution (0.04 M).

Firstly, the influences of the solution pH on Nafion/SAP/HRP/Au-GN/GCE were investigated by tuning the pH of the B-R buffer solution. As seen in Fig. S4A, the LSV presents stable and well-defined peak in the acidity of pH 2.0 (curve a), but the anodic peak disappeared and the base line rose up with the increase of pH from 3

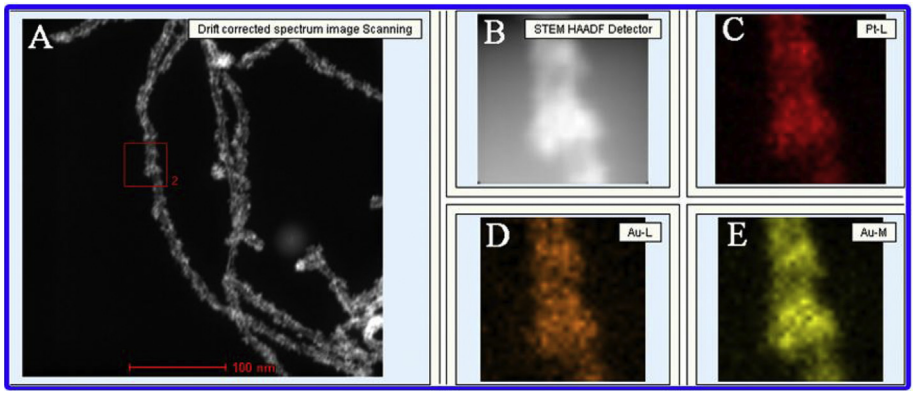

Fig. 2. **(A)** HAADF–STEM images and **(B)** the selected–area (the red labeled part in **A**) of spiny Pt-Au NTs. **(C)**, **(D)** and **(E)** HAADF–STEM energy–dispersive X–ray spectroscopy (EDX) mapping image of spiny Pt-Au NTs. (For interpretation of the references to colour in this figure legend, the reader is referred to the web version of this article.)

to 11 (curve b to g). Thus, the optimum pH was chosen as 2.0 to perform the following experiments. Subsequently, the concentration of HRP and SAP NTs were explored as shown in Fig. S5. It can be seen that the best analytical signal for HRP (Fig. S5A) and SAP NTs (Fig. S5B) was 5.0 mg L^{-1} and 5.0 mM, respectively. Also, we discussed the H_2O_2 concentration on the LSV process because HRP requires hydrogen peroxide to catalyse the reaction. From Fig. S4B, it can be found that the optimum concentration was 1.0 mM. Finally, the scan rate was studied to reveal the behavior of the modified electrode. It is observed that the redox peaks changed upon the scan rate (Fig. 3A), and the cathodic peak currents and the anodic peak currents increase linearly with the increase of square-root of scan rate ($v^{1/2}$) (Fig. 3B). These results indicate that the electrochemical behavior of PG on the modified electrode is a typical diffusion-controlled process. Therefore, the above experimental conditions were used in subsequent experiments.

3.3. Electrochemical characterization of SAP NTs

The electrochemical performance of the SAP NTs was investigated by CV and electrochemical impedance spectroscopy (EIS). As depicted in Fig. S6A, the CVs of different electrodes were performed in a 5.0 mM $K_3[Fe(CN)_6]$ with 0.5 M KCl. Bare GCE (curve a) behaved two well-defined redox peaks corresponding to $[Fe(CN)_6]^{3-/4-}$, revealing the good electron transfer interface. Moreover, after the GCE was fabricated with a layer of Nafion/Au-GN film, the redox peak behaves great enhancement (curve b), which implied that the electron transfer at the electrode surface was accelerated due to the good conductivity of Au-GN. However, when Nafion/HRP/Au-GN/GCE was tested at same conditions (curve c), the peaks decreased to a great extent, which indicated the electrode surface was blocked due to the interior conductivity of HRP. Meanwhile, the CV of Nafion/SAP/HRP/Au-GN/GCE was also recorded (curve d). The result indicated that the redox peak was enhanced again, which means that SAP NTs have great effects on the improving the electrochemical property of the electrode.

EIS is an effective method to probe the interface property of the electrode modified with different substances. The assembly process of the modified electrode was further characterized by EIS as shown in Fig. S6B. It was observed that the bare GCE revealed a small semicircle portion (curve a). Subsequently, the Nafion/Au-GN/GCE showed a lower resistance (curve b), implying that Au-GN was an excellent electric conducting material and accelerated the electron transfer. For the HRP modified step (curve c), Nafion/HRP/Au-GN/GCE generated an insulating protein layer resultant with a higher resistance. However, the electron-transfer resistance decreased greatly when SAP NTs were further assembled onto HRP/Au-GN composite film (curve d). The facts were consistent with the results obtained by CV, indicating that the electrode was fabricated as expected.

3.4. LSV characterization assays

Under the above optimized conditions, calibration curves for BHA and PG were made using LSV and the proposed biosensor. The oxidation potentials of BHA and PG at the biosensor surface were observed at 624 mV (Fig. 3C) and 655 mV (Fig. 3D), respectively. Furthermore, it can be found that the current peaks versus BHA concentrations displayed a wide linear response between 0.3 and 50 mg L^{-1}, and PG concentrations from 0.1 to 100 mg L^{-1}. The results can be put as the following equations: $\Delta i = 5.266 + 1.228$ [BHA] (mg L^{-1}) and $\Delta i = 3.295 + 0.674$ [PG] (mg L^{-1}) with a correlation coefficient of 0.9982 and 0.9985, where Δi is the peak current (μA). The detection limits (LOD) were calculated to be 0.046 and 0.024 mg L^{-1} (3σ/slope), respectively. The proposed method was compared with that of others in previously published reports (Table 1). Furthermore, to demonstrate the detection results of BHA and PG, a simple visual detection method was developed by using

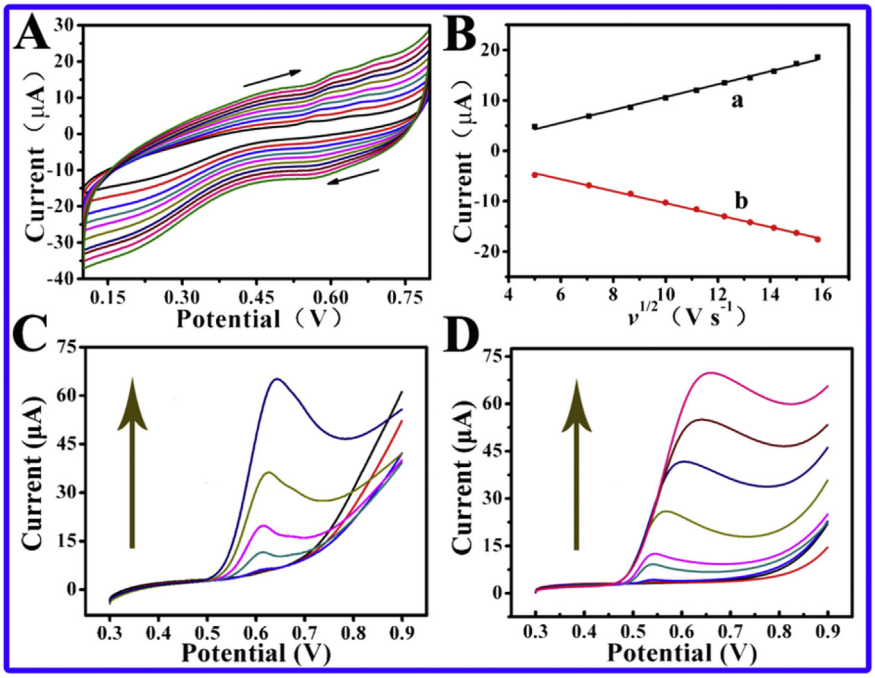

Fig. 3. **(A)** Cyclic voltammograms of the Nafion/SAP/HRP/Au-GN/GCE in 0.04 M Britton–Robinson (B–R) buffer solution (pH = 2) at different scan rates (from inner to outer): 25, 50, 75, 100, 125, 150, 175, 200, 225, 250 mV/s. **(B)** Linear relationship of cathodic (a) and anodic (b) peak currents versus square-root of scan rate ($v^{1/2}$). LSV response to different concentrations of **(C)** BHA (from bottom to up: 0.3, 0.5, 1.0, 5.0, 10, 30, 50 mg L^{-1}) **(D)** and PG (from bottom to up: 0.3, 0.5, 1.0, 5.0, 10, 30, 50, 80, 100 mg L^{-1}) using SAP/HRP/Au-GN/GCE.

Table 1
Comparison of the proposed method with other methods for BHA and PG detection (unit: mg L^{-1}).

Detection technique	Linear range		Detection limit		Reference
	BHA	PG	BHA	PG	
HPLC–CL[a]	0.1–10	–	0.033	–	[38]
HPLC–FLD[b]	0.28–2.84	3.14–31.36	0.0097	0.193	[13]
MECC–ED[c]	0.90–90	0.42–106.1	0.18	0.62	[39]
SPEs–DPV[d]	0.2–2.1	0.2–2.1	0.093	0.022	[40]
CE–AD[e]	1.8–180.2	10.6–212.2	1.4	1.1	[41]
LSV	0.10–1.50	–	0.039	–	[35]
LSV	0.5–15.0	1.0–15.0	0.19	0.54	[6]
LSV	0.3–50	0.1–100	0.046	0.024	This work

[a] HPLC coupled with chemiluminescence.
[b] HPLC with fluorescence detector.
[c] Micellar electrokinetic capillary chromatography method with electrochemical detection.
[d] Screen-printed electrodes with differential pulse voltammetry.
[e] Capillary electrophoresis-amperometric determination.

ASP NTs as catalyst and TMB as indicator. Due to the good antioxidant activity of BHA and PG, it can be clearly seen (Fig. 4A and B) that the optical density increases with the decrease of BHA and PG concentrations, and both of them behaved linear response to the optical density. The dependent linear equations are listed in Table S1 and the results revealed that the visual analysis were consistent with the proposed LSV method. Also, the chromogenic reaction of TMB showed that ASP NTs exhibited intrinsic peroxidase activity. Moreover, the catalytic properties of ASP NTs towards BHA and PG were also discussed in Fig. S7. The results showed that ASP NTs behaved good catalytic properties towards BHA, especially for PG.

To further verify the precision of the method, the repeatability and reproducibility were demonstrated with intra-assay and inter-assay by measuring one concentration (100 mg L^{-1}) using LSV for six measurements. The variation coefficients of intra- and inter-assay for BHA and PG were 4.6%, 3.8% and 5.2%, 4.5%, indicating the acceptable reproducibility of the proposed biosensor. Moreover, the biosensor stability was tested in a mixture solution of BHA and PG over a period of 10 weeks (Fig. S8). It was found that the current response showed normal random fluctuations within the limits of statistical control, revealing the acceptable stability of the biosensor.

3.5. Analysis of food samples

The proposed method was applied for detecting BHA and PG mixture in several commercial food products according to the procedures described in the experimental section and by using standard addition method. Firstly, different concentrations of standard mixture solutions were prepared and the results were recorded by LSV (Fig. 4C). The results showed that the current response behaved stable increase with the increase of concentration in accordance with the above detection range and the oxidation peak of BHA and PG exhibited well-defined single oxidation peak at 624 mV and 655 mV, respectively. All the facts are consistent with the results in Fig. 3, suggesting the feasibility of simultaneous detection of BHA and PG. To further verify the specificity of the proposed method to real samples detection, the interference such as TBHQ, BHA and BPA were investigated as shown in Fig. 4D. As can be seen, the oxidation peak became wider when the interferences were introduced but the current response and oxidation potential nearly remained the same with Fig. 4C. The results revealed that the proposed method behave stable current towards BHA and PG mixture even in the presence of interferences, indicating the acceptable specificity of the biosensor in simultaneous detection of BHA and PG.

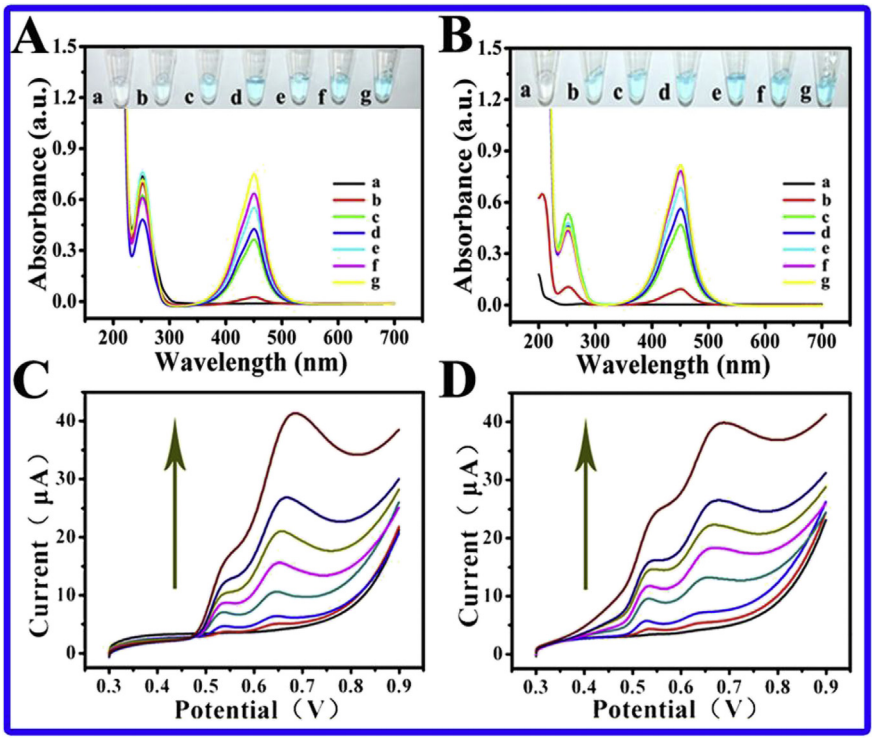

Fig. 4. The evolution of optical density upon different concentrations of **(A)** BHA (from a to g: 6, 3, 1.5, 0.6, 0.3, 0.15, 0 mg L^{-1}) and **(B)** PG (from a to g: 3, 1.5, 0.75, 0.3, 0.15, 0.075, 0 mg L^{-1}) with TMB (6 mM) and SAP NTs. **(C)** LSV responses to different concentrations of BHA and PG mixture (from bottom to up: 0.1, 0.5, 1.0, 3.0, 5.0, 8.0, 10, 20 mg L^{-1}) based on the biosensors. **(D)** Verification of the biosensors after adding TBHQ, BHT and BPA under the same concentration.

Also, standard addition method was adopted to analyze food samples and the responses do not differ from that for standard samples. Thus, it is verified again that the biosensors behaved excellent specificity and stability. Since the concentration of both antioxidants in food samples were previously known (the analyses had been dealt with spiked samples), it was possible to evaluate the accuracy and precision of all the results by calculating recovery and relative standard deviation (RSD). As shown in Table S2, four kinds of food matrixes were evaluated and no BHA or PG was found in the extraction samples. After the addition of BHA and PG, the recovery and RSD of the method exhibited the range of 87.3–126.2% and 3.4–5.8%, respectively, which was comparable to those achieved using HPLC method (Table S3, Fig. S9), which demonstrated that the approach was satisfactory for the quantitative determination of BHA and PG in food samples.

4. Conclusions

In this work, spiny Au-Pt nanotubes with good catalytic performance were prepared, based on which an enzymatic biosensor has been constructed for the simultaneous determination of BHA and PG in food matrices using LSV method. The biosensor displayed excellent analytical performance to BHA and PG with a wide linear range of 0.3–50 mg L^{-1} and 0.1–100 mg L^{-1}, respectively. The sensitivity for BHA and PG were 0.046 mg L^{-1} and 0.024 mg L^{-1} (3σ/slope), respectively. Moreover, interferences from TBHQ, BHT and BPA were almost negligible to the BHA and PG detection. Furthermore, a visual detection method was developed to demonstrate the feasibility of the proposed strategy. Finally, recovery experiments revealed that the recovery and RSD showed the range of 87.3–126.2% and 3.4–5.8%, which was comparable to those achieved using HPLC method. Overall, this report provides a new method in the simultaneous detection of BHA and PG with good sensitivity, stability and reproducibility, and can provide an alternative for electrode fabricating and the construction of sensitive biosensors.

Acknowledgment

We gratefully acknowledge the financial support from National Natural Science Foundation of China (21375043, 21175051).

Appendix A. Supplementary data

Supplementary data related to this article can be found at http://dx.doi.org/10.1016/j.aca.2016.06.020.

References

[1] M. Carocho, I.C.F.R. Ferreira, A review on antioxidants, prooxidants and related controversy: natural and synthetic compounds, screening and analysis methodologies and future perspectives, Food Chem. Toxicol. 51 (2013) 15–25.
[2] S. Rashid, M.A. Rather, W.A. Shah, B.A. Bhat, Chemical composition, antimicrobial, cytotoxic and antioxidant activities of the essential oil of artemisia indica willd, Food Chem. 138 (2013) 693–700.
[3] E.S. Almeida, F.M. Portela, R.M.F. Sousa, D. Daniel, M.G.H. Terrones, E.M. Richter, Behaviour of the antioxidant tert-butylhydroquinone on the storage stability and corrosive character of biodiesel, Fuel 90 (2011) 3480–3484.
[4] M. Tomášková, J. Chýlková, T. Navrátil, R. Šelešovská, Voltammetric determination of TBHQ individually and mixed with BHT in petroleum products using a gold disc electrode, Energy Fuels 28 (2014) 4731–4736.
[5] J.G. Chung, Effects of butylated hydroxyanisole and butylated hydroxytoluene on the acetylation of 2-aminofluorene and DNA-2-aminofluorene adducts in the rat, Toxicol. Sci. 51 (1999) 202–210.
[6] Y. Ni, L. Wang, S. Kokot, Voltammetric determination of butylated hydroxyanisole, butylated hydroxytoluene, propyl gallate and tert-butylhydroquinone by use of chemometric approaches, Anal. Chim. Acta 412 (2000) 185–193.
[7] P. Zhao, J. Hao, Tert-butylhydroquinone recognition of molecular imprinting electrochemical sensor based on core–shell nanoparticles, Food Chem. 139 (2013) 1001–1007.
[8] H. Kobayashi, S. Oikawa, K. Hirakawa, S. Kawanishi, Metal-mediated oxidative damage to cellular and isolated DNA by gallic acid, a metabolite of antioxidant propyl gallate, Mutat. Res. 558 (2004) 111–120.
[9] M.Z. Ding, J.K. Zou, Rapid micropreparation procedure for the gas chromatographic–mass spectrometric determination of BHT, BHA and TBHQ in edible oils, Food Chem. 131 (2012) 1051–1055.
[10] R. Rodila, J.B. Quintana, G. Basaglia, M.C. Pietrogrande, R. Cela, Determination of synthetic phenolic antioxidants and their metabolites in water samples by downscaled solid-phase extraction, silylation and gas chromatography–mass spectrometry, J. Chromatogr. A 1217 (2010) 6428–6435.
[11] C. André, I. Castanheira, J.M. Cruz, P. Paseiro, A. Sanches-Silva, Analytical strategies to evaluate antioxidants in food: a review, Trends Food Sci. Technol. 21 (2010) 229–246.
[12] T.A. Araujo, A.M.J. Barbosa, L.H. Viana, V.S. Ferreira, Electroanalytical determination of TBHQ, a synthetic antioxidant, in soybean biodiesel samples, Fuel 90 (2011) 707–712.
[13] J.Y. Wang, H.L. Wu, Y.M. Sun, H.W. Gu, Z. Liu, Y.J. Liu, R.Q. Yu, Simultaneous determination of phenolic antioxidants in edible vegetable oils by HPLC–FLD assisted with second-order calibration based on ATLD algorithm, J. Chromatogr. B 947 (2014) 32–40.
[14] R.L. Webster, P.M. Rawson, D.J. Evans, P.J. Marriott, Synthetic phenolic antioxidants in middle distillate fuels analyzed by gas chromatography with triple quadrupole and quadrupole time-of-flight mass spectrometry, Energy Fuels 28 (2014) 1097–1102.
[15] P. Biparva, M. Ehsani, M.R. Hadjmohammadi, Dispersive liquid–liquid microextraction using extraction solvents lighter than water combined with High performance liquid chromatography for determination of synthetic antioxidants in fruit juice samples, J. Food Compos. Anal. 27 (2012) 87–94.
[16] J. Tabart, C. Kevers, J. Pincemail, J.O. Defraigne, J. Dommes, Evaluation of spectrometric methods for antioxidant compound measurement in relation to total antioxidant capacity in beverages, J. Food Chem. 120 (2010) 607–614.
[17] L. Wu, X. Li, K. Shao, S. Ye, C. Liu, C. Zhang, H. Han, Enhanced immunoassay for porcine circovirus type 2 antibody using enzyme-loaded and quantum dots-embedded shell–core silica nanospheres based on enzyme-linked immunosorbent assay, Anal. Chim. Acta 887 (2015) 192–200.
[18] X. Lv, W. Ge, Q. Li, Y. Wu, H. Jiang, X. Wang, Rapid and ultrasensitive electrochemical detection of multidrug-resistant bacteria based on nanostructured gold coated ITO electrode, ACS Appl. Mater. Interfaces 6 (2014) 11025–11031.
[19] S. Ignatov, D. Shishniashvili, B. Ge, F.W. Scheller, F. Lisdat, Amperometric biosensor based on a functionalized gold electrode for the detection of antioxidants, Biosens. Bioelectron. 17 (2002) 191–199.
[20] M.F. Barroso, C. Delerue-Matos, M.B.P.P. Oliveira, Towards a reliable technology for antioxidant capacity and oxidative damage evaluation: electrochemical (bio) sensors, Biosens. Bioelectron. 26 (2011) 3748–3754.
[21] H. Gao, X. Qi, Y. Chen, W. Sun, Electrochemical deoxyribonucleic acid biosensor based on the self-assembly film with nanogold decorated on ionic liquid modified carbon paste electrode, Anal. Chim. Acta 704 (2011) 133–138.
[22] J. Yan, V.A. Pedrosa, A.L. Simonian, A. Revzin, Immobilizing enzymes onto electrode arrays by hydrogel photolithography to fabricate multi-analyte electrochemical biosensors, ACS Appl. Mater. Interfaces 2 (2010) 748–755.
[23] I.R.W.Z. de Oliveira, I.C. Vieira, Immobilization procedures for the development of a biosensor for determination of hydroquinone using chitosan and Gilo (Solanum gilo), Enzyme Microb. Technol. 38 (2006) 449–456.
[24] T.R. de Oliveira, G.F. Grawe, S.K. Moccelini, A.J. Terezo, M. Castilho, Enzymatic biosensors based on Inga-cipo peroxidase immobilised on sepiolite for TBHQ quantification, Analyst 139 (2014) 2214–2220.
[25] J. Li, J. Xie, L. Gao, C.M. Li, Au Nanoparticles–3D graphene hydrogel nanocomposite to boost synergistically in situ detection sensitivity toward cell-released nitric oxide, ACS Appl. Mater. Interfaces 7 (2015) 2726–2734.
[26] S.K. Vashist, J.H.T. Luong, Recent advances in electrochemical biosensing schemes using graphene and graphene-based nanocomposites, Carbon 84 (2015) 519–550.
[27] T.T. Baby, S.S.J. Aravind, T. Arockiadoss, R.B. Rakhi, S. Ramaprabhu, Metal decorated graphene nanosheets as immobilization matrix for amperometric glucose biosensor, Sens. Actuators B Chem. 145 (2010) 71–77.
[28] X.H. Kang, Z.B. Mai, X.Y. Zou, P.X. Cai, J.Y. Mo, A novel glucose biosensor based on immobilization of glucose oxidase in chitosan on a glassy carbon electrode modified with gold–platinum alloy nanoparticles/multiwall carbon nanotubes, Anal. Biochem. 369 (2007) 71–79.
[29] L. Wu, W. Yin, K. Tang, K. Shao, Q. Li, P. Wang, Y. Zuo, X. Lei, Z. Lu, H. Han, Highly sensitive enzyme-free immunosorbent assay for porcine circovirus type 2 antibody using Au-Pt/SiO_2 nanocomposites as labels, Biosens. Bioelectron. 82 (2016) 177–184.
[30] L. Usón, V. Sebastian, A. Mayoral, J.L. Hueso, A. Eguizabal, M. Arrueboab, Spontaneous formation of Au-Pt alloyed nanoparticles using pure nanocounterparts as starters: a ligand and size dependent process, Nanoscale 7 (2015) 10152–10161.
[31] L. Wu, K. Chen, Z. Lu, T. Li, K. Shao, F. Shao, H. Han, Hydrogen-bonding recognition-induced aggregation of gold nanoparticles for the determination of the migration of melamine monomers using dynamic light scattering, Anal. Chim. Acta 845 (2014) 92–97.
[32] J. Wang, H. Han, X. Jiang, L. Huang, L. Chen, N. Li, Quantum dot-based near-

infrared electrochemiluminescent immunosensor with gold nanoparticle-graphene nanosheet hybrids and silica nanospheres double-assisted signal amplification, Anal. Chem. 84 (2012) 4893–4899.
[33] K. Shao, J. Wang, X. Jiang, F. Shao, T. Li, S. Ye, L. Chen, H. Han, Stretch-stowage-growth strategy to fabricate tunable triply-amplified electrochemiluminescence immunosensor for ultrasensitive detection of pseudorabies virus antibody, Anal. Chem. 86 (2014) 5749–5757.
[34] J. Che, P. Chen, M.B. Chen-Park, High-strength carbon nanotube buckypaper composites as applied to free-standing electrodes for supercapacitors, J. Mater. Chem. A 1 (2013) 4057–4066.
[35] X. Lin, Y. Ni, S. Kokot, Glassy carbon electrodes modified with gold nanoparticles for the simultaneous determination of three food antioxidants, Anal. Chim. Acta 765 (2013) 54–62.
[36] X. Lu, Q. Zhang, L. Zhang, J. Li, Direct electron transfer of horseradish peroxidase and its biosensor based on chitosan and room temperature ionic liquid, Electrochem. Commun. 8 (2006) 874–878.
[37] C. Xu, R. Wang, M. Chen, Y. Zhang, Y. Ding, Dealloying to nanoporous Au/Pt alloys and their structure sensitive electrocatalytic properties, Phys. Chem. Chem. Phys. 12 (2010) 239–246.
[38] S. Xu, F. Chen, M. Deng, Y. Sui, Simple simultaneous determination of butylated hydroquinone (TBHQ) and butylated hydroxyanisole (BHA) antioxidants in oil using high-performance liquid chromatography with chemiluminescence detection, Luminescence 29 (2014) 1027–1032.
[39] Y. Guan, Q. Chu, L. Fu, T. Wu, J. Ye, Determination of phenolic antioxidants by micellar electrokinetic capillary chromatography with electrochemical detection, Food Chem. 94 (2006) 157–162.
[40] R.P. Caramit, A.S.A. Araújo, D.K. Fogliatto, L.H. Viana, M.A.G. Trindade, V.S. Ferreira, Carbon-nanotube-modified screen-printed electrodes, a cationic surfactant, and a peak deconvolution procedure: alternatives to provide satisfactory simultaneous determination of three synthetic antioxidants in complex samples, Anal. Methods 7 (2015) 3764–3771.
[41] Q. Xiang, Y. Gao, Y. Xu, E. Wang, Capillary electrophoresis-amperometric determination of antioxidant propyl gallate and butylated hydroxyanisole in foods, Anal. Sci. 23 (2007) 713–717.